2013 European Control Conference (ECC)
July 17-19, 2013, Zürich, Switzerland.

Robust Vehicle Stability Control with an Uncertain Driver Model

Ashwin Carvalho†, Giovanni Palmieri*, H. Eric Tseng♯, Luigi Glielmo*, Francesco Borrelli†

Abstract— **We present the design of a robust lateral stability controller to track yaw rate and lateral velocity reference signals while avoiding front and rear tire force saturation. The controller takes into account the driver's intent at the design stage by treating it as a measured disturbance. The uncertainty in the driver's input is modeled as a set–valued function of the vehicle states. The control design is based on a hybrid piecewise affine bicycle model with input–dependent and state–dependent uncertainties. The performance of the controller and the importance of driver behavior modeling are demonstrated through experimental tests on ice with aggressive driver maneuvers.**

I. Introduction

Modern passenger vehicles are equipped with active safety systems which assist drivers in order to stabilize the vehicle and prevent accidents. In this work, we focus on the integration of two active safety systems, Electronic Stability Control (ESC) and Active Front Steering (AFS), which enhance vehicle stability by applying braking torques to the wheels and correcting the front steering, respectively [1], [2]. This problem has been studied in the past by several authors. For instance, optimal control methods have been studied in [3], generalized predictive control in [4] and state feedback linearization in [5]. In [6], [7], the authors of the present work presented a model–based predictive control technique in which a piecewise affine (PWA) vehicle dynamics model was used for the control design.

Four elements make the control problem nontrivial: the vehicle model uncertainty, the nonlinear tire characteristics, the presence of state and input constraints, and the uncertainty in driver behavior. We present a systematic approach to design a robust lateral stability controller which addresses all four challenges in a unified framework during the control design process. In particular, the nonlinear vehicle dynamics are modeled as a PWA system in which the states and inputs are subject to hard constraints. Model mismatch is captured by introducing an additive uncertainty in the input. Finally, the driver's steering input is treated as a bounded disturbance in the model, whose bounds are a set–valued function of the vehicle states.

The principal goal of our control strategy is to enlarge the vehicle's stability region when it undertakes aggressive maneuvers. Such maneuvers are primarily determined by the front wheel steering angle which is a combined effect of the driver's steering input and the AFS correction. In order to take both contributions into account, we propose the use of a predictive control framework which considers the driver's input as a measured disturbance, and the AFS correction as a constrained control input. Our main motivation is to ensure robustness to the uncertainty in the driver's inputs at each time step. In this work, we extend the methodology presented in [7] to account for this uncertainty.

We use set–theoretic methods for the control synthesis [9]. The theoretical framework developed in [7] forms the basis for our control design. In particular, we compute the robust control invariant (RCI) set for the PWA vehicle model using results on min–max and max–min reachability [9]–[11]. Such a RCI set constitutes the target set of a robust time–optimal control algorithm. Experimental tests at high speeds on ice with aggressive driver maneuvers show the effectiveness of the proposed scheme.

The paper is structured as follows. Section II describes the derivation of the PWA model starting from the nonlinear bicycle model. The construction of the set–valued bounds on the driver steering is also shown. In Section III, we discuss the theoretical framework used for the design of the robust controller. We present experimental results in Section IV, followed by final remarks in Section V.

II. Vehicle Model

The following notation is introduced: $(\cdot)_f$ and $(\cdot)_r$ denote variables associated with the front and the rear wheels, respectively. $(\cdot)_\star$ is used to refer to both wheels.

A. PWA hybrid model

The classical nonlinear bicycle model [12], [13] is given by

$$m\ddot{y} = -m\dot{x}\dot{\psi} + 2F_{c_f} + 2F_{c_r}, \tag{1a}$$

$$I\ddot{\psi} = 2aF_{c_f} - 2bF_{c_r} + M, \tag{1b}$$

where $\dot{y}$ is the lateral speed, $\dot{x}$ is the longitudinal velocity, $\dot{\psi}$ is the yaw rate, M is the external yaw moment, $F_{c_\star}$ are the lateral cornering forces, a and b are the distances from the vehicle center of gravity to the front and rear axle, respectively, and I is the moment of inertia of the vehicle about the z-axis. The notation used is depicted in Figure 1.

The lateral tire forces $F_{c_\star}$ are given by the Pacejka model [14], and are nonlinear functions of the tire slip angles $\alpha_\star$, slip ratios $\sigma_\star$, normal forces $F_{z_\star}$ and friction coefficient between the tire and road $\mu_\star$. That is,

$$F_{c_\star} = f_{c,\star}(\alpha_\star, \sigma_\star, F_{z_\star}, \mu_\star). \tag{2}$$

The nonlinear relationship between the lateral force and the wheel slip angle (for $\sigma = 0$), and its PWA approximation are

† Department of Mechanical Engineering,University of California, Berkeley, CA 94720-1740, USA
*Engineering Department, Universitá degli Studi del Sannio, 82100 Benevento, Italy
♯ Powertrain Control R&A, Ford Motor Company, Dearborn, MI, U.S.A.

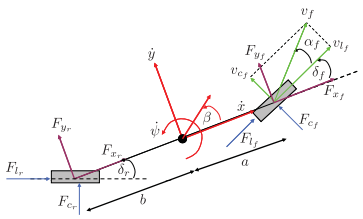

Fig. 1. Schematic of bicycle model of vehicle [7].

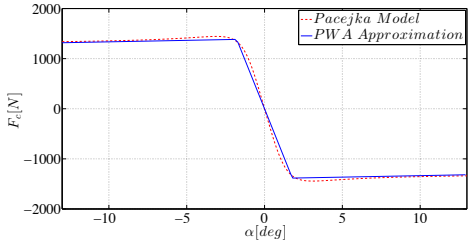

Fig. 2. Lateral tire forces and the PWA approximation [7].

depicted in Figure 2. We introduce the following assumptions to derive the PWA model approximating (1).

Assumption 1: The friction coefficient μ and the normal force F_z are known, constant and identical for both wheels.

Assumption 2: The longitudinal velocity $\dot{x}$ is known and constant. The longitudinal vehicle dynamics are ignored, and $\sigma_\star$ is assumed to be zero (pure cornering).

Under these assumptions, $F_{c_\star}$ is only a function of $\alpha_\star$. Using the small angle approximation and assuming zero rear wheel steering, $\alpha_\star$ can be expressed as a linear function of the states and inputs [13], [14]:

$$\alpha_f = \frac{\dot{y} + a\dot{\psi}}{\dot{x}} - \delta_f, \qquad \alpha_r = \frac{\dot{y} - b\dot{\psi}}{\dot{x}}, \tag{3}$$

where δ_f is the front wheel steering angle relative to the longitudinal axis of the vehicle. The PWA approximation of the nonlinear function $f_{c,\star}(\cdot)$ in (2) is given by

$$f^{pwa}_{c,\star}(\alpha_\star) = \begin{cases} c_s\alpha_\star + (c_l + c_s)\hat{\alpha}_\star & \text{if } \alpha_\star \le -\hat{\alpha}_\star, \\ -c_l\alpha_\star & \text{if } -\hat{\alpha}_\star \le \alpha_\star \le \hat{\alpha}_\star, \\ c_s\alpha_\star - (c_l + c_s)\hat{\alpha}_\star & \text{if } \alpha_\star \ge \hat{\alpha}_\star, \end{cases} \tag{4}$$

where c_l and c_s are the cornering stiffnesses of the tires in the linear and saturated regions, respectively, and $\hat{\alpha}_\star$ is the slip angle at which the lateral force is maximum. The hybrid bicycle model is obtained by combining (1), (3) and (4), and can be written as

$$\begin{bmatrix} \ddot{y} \\ \ddot{\psi} \end{bmatrix} = A_i \begin{bmatrix} \dot{y} \\ \dot{\psi} \end{bmatrix} + B_i \begin{bmatrix} \delta_f \\ M \end{bmatrix} + f_i, \quad (i = 1, 2, ..., 9). \tag{5}$$

Model (5) has nine modes resulting from all possible combinations of the three modes for the front wheels and the three modes for the rear wheels. It is important to note that in a vehicle equipped with an AFS system, the front wheel steering angle δ_f is the sum of the steering angles resulting from two independent inputs: (*i*) the driver's input at the steering wheel, and (*ii*) the AFS input. That is,

$$\delta_f = \delta_d + \delta_{AFS}. \tag{6}$$

We also introduce an additive uncertainty w_u in the input to account for unmodeled actuator dynamics and input delays. The modified PWA bicycle model can then be written in a discrete–time state–space form as

$$z(k+1) = A^d_i z(k) + B^d_i u(k) + W^d_i \delta_d(k) + f^d_i + B^d_i w_u, \tag{7}$$
$$(z, u, \delta_d) \in \mathcal{Q}_i \quad (i = 1, 2, ..., 9), \qquad w_u \in \mathcal{W}_u(u),$$

where $z := [\dot{y}, \dot{\psi}]^T$ and $u := [\delta_{AFS}, M]^T$. $\{\mathcal{Q}_i\}_{i=1}^9$ is a collection of polyhedral regions which defines the state and input constraints corresponding to the nine modes of the vehicle, and $\mathcal{W}_u(\cdot)$ is a set–valued mapping which defines bounds on w_u. The regions $\mathcal{Q}_i$ are obtained from the slip angle inequalities associated with each of the cases in (4). Note that $\mathcal{W}_u(\cdot)$ is defined to be a set–valued function as the uncertainty in the input may depend on its value. In this paper, we assume an uncertainty of 10% in each of the control inputs.

Reformulating (5) as (7) has several advantages:

- It allows us to impose bounds (arising from design constraints) directly on δ_{AFS} as opposed to imposing bounds on δ_f. This ensures that the input commanded by the controller can actually be attained.
- It enables us to guarantee vehicle stability for any anticipated behavior of the driver. This is achieved by treating δ_d in (7) as a measured disturbance which is bounded by a function of the vehicle states. We design the controller to be robust to this disturbance.

B. Uncertain driver model

In this section, we construct constraints of the form $\delta_d \in \mathcal{W}_z(z)$, where $\mathcal{W}_z(\cdot)$ is a set–valued mapping of the state z. Conservative bounds on δ_d can be obtained by assuming a worst–case scenario. We derive less conservative bounds on δ_d based on a steady–state cornering analysis of the linear bicycle model [13], [15]. At steady–state, the relationship between $\dot{\psi}$ and δ_f is given by:

$$\dot{\psi}_{ss} = \frac{v_x}{l(1 + v_x^2/v_{ch}^2)}\delta_{f,ss} =: \frac{\delta_{f,ss}}{K_{\psi,ss}} =: G_{\psi,ss}\delta_{f,ss}, \tag{8}$$

where $l = a + b$, $v_x = \dot{x}$ and v_{ch} is the characteristic speed [13]. $G_{\psi,ss} := 1/K_{\psi,ss}$ represents the steady–state yaw rate gain. Inverting (8) and assuming no control ($\delta_{AFS,ss} = 0$) at steady–state gives

$$\delta_{f,ss} = \delta_{d,ss} = K_{\psi,ss}\dot{\psi}_{ss}. \tag{9}$$

We use the value of $\delta_{d,ss}$ obtained from (9) as a linear state–dependent estimate of the driver's steering input. We then assume that the actual value of δ_d lies in an interval centered at $\delta_{d,ss}$. Thus,

$$\mathcal{W}_z(z) = \left\{\delta_d : |\delta_d - K_{\psi,ss}\dot{\psi}| \le \epsilon, |\delta_d| \le \delta_{d,max}\right\}, \tag{10}$$

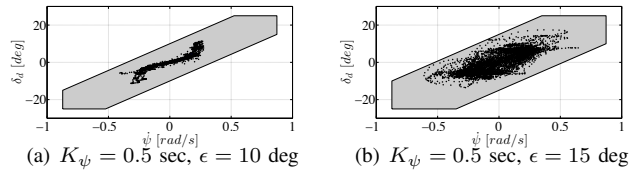

(a) $K_\psi = 0.5$ sec, $\epsilon = 10$ deg (b) $K_\psi = 0.5$ sec, $\epsilon = 15$ deg

Fig. 3. State–dependent constraints on δ_d validated with data from different sets of experiments and the same driver.

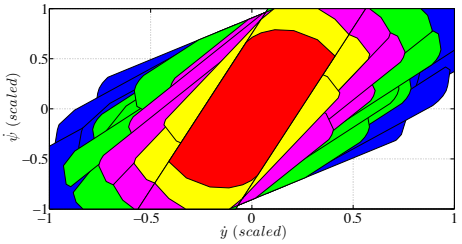

Fig. 4. 4–step controllable sets to $\mathcal{Z}^1_\infty$, $\mu = 0.3$, $v_x = 50$ kph. The different colors correspond to the various steps.

where ϵ is a non–negative parameter which must be chosen. The constraint $\delta_d \in \mathcal{W}_z(z)$ can also be expressed in terms of a polytopic constraint in $\mathbb{R}^3$. That is,

$$\delta_d \in \mathcal{W}_z(z) \Leftrightarrow (z, \delta_d) \in \mathcal{W}_d \subseteq \mathbb{R}^3. \tag{11}$$

Note that the bounds on δ_d are derived assuming the vehicle is cornering in a steady–state condition. Therefore, in practice, the average gain $(\delta_d/\dot{\psi})$ differs from $K_{\psi,ss}$. We account for this by using a modified gain K_ψ in (10). This is illustrated in Figure 3, in which we plot the values of δ_d vs $\dot{\psi}$ obtained from experimental tests. The empirical value of K_ψ was computed to be $K_\psi \approx 0.5$ sec. The projection of the polytope $\mathcal{W}_d$ defined in (11) on the δ_d–$\dot{\psi}$ space is also plotted in Figure 3. Note that the choice of K_ψ and ϵ is critical to our analysis. For example, in Figure 3(b), a higher value of ϵ is needed to ensure constraint satisfaction. The choice of ϵ is a trade–off between being too conservative on one hand, and having the possibility of violating constraints on the other.

III. Robust Control Design

The objective of the robust stability control system is to keep the front and rear tires in the linear region *for all admissible values* of δ_d and w_u. This linear mode of the vehicle is denoted as "Mode 1". If the vehicle goes outside mode 1, we want the controller to compute a feasible input which ensures that the vehicle goes back into mode 1 in a finite number of time steps. Moreover, when the vehicle is in mode 1, the controller action should be such that the predicted state at the next time step should also lie in mode 1. These notions of *reaching* a specified *target set* in the state–space and *staying* within the target set *for all admissible values of the disturbance variables* can be formalized using the framework of robust reachability analysis [9], [16].

A. Robust reachability framework

We make use of the notion of robust controllable or backward reachable sets which are defined below.

Definition 1: The *one–step robust backward reachable set* to a given target set $\mathcal{Z}$ in the state–space is defined as:

$$Pre(\mathcal{Z}) := \{z : \forall \delta_d \in \mathcal{W}_z(z), \exists u \text{ such that } (z, u, \delta_d) \in \mathcal{Q}, z^+ \in \mathcal{Z}, \forall w_u \in \mathcal{W}_u(u)\}, \tag{12}$$

where z^+ is the predicted state at the next time step given by (7) and $\mathcal{Q} := \bigcup_{i=1}^9 \mathcal{Q}_i$.
The $Pre(\cdot)$ mapping gives us the set of states from which there exists at least one feasible input that can ensure that the predicted state is inside the target set, for all admissible values of the disturbances δ_d and w_u. In addition to the one–step controllable sets, we introduce the notions of the robust control invariant (RCI) set associated with mode 1, and the corresponding control mapping. Let $\mathcal{P}_1 = \text{Proj}_z(\mathcal{Q}_1)$, where $\mathcal{Q}_1 \subseteq \mathbb{R}^5$ defines the state and input constraints for mode 1.

Definition 2: A set $\mathcal{Z}^1_i \subseteq \mathcal{P}_1$ is called a *mode 1 RCI set* if for every $z \in \mathcal{Z}^1_i$ and each $\delta_d \in \mathcal{W}_z(z)$, there exists a control u such that $(z, u, \delta_d) \in \mathcal{Q}_1$ and $z^+ \in \mathcal{Z}^1_i$, for all $w_u \in \mathcal{W}_u(u)$.

Definition 3: The *maximal mode 1 RCI set* $\mathcal{Z}^1_\infty$ is the RCI set which contains all mode 1 RCI sets $\mathcal{Z}^1_i$.

Definition 4: The *control mapping* $\mathcal{U}^1_\infty(\cdot)$ *corresponding to* $\mathcal{Z}^1_\infty$ is defined as

$$\mathcal{U}^1_\infty(z, \delta_d) := \{u : (z, u, \delta_d) \in \mathcal{Q}_1, z^+ \in \mathcal{Z}^1_\infty, \forall w_u \in \mathcal{W}_u(u)\}. \tag{13}$$

If the state z of the vehicle lies in $\mathcal{Z}^1_\infty$, then for each $\delta_d \in \mathcal{W}_z(z)$, any choice of input u from $\mathcal{U}^1_\infty(z, \delta_d)$ would cause the predicted state at the next time step to remain in $\mathcal{Z}^1_\infty$. However, it is possible for the state of the vehicle to go outside $\mathcal{Z}^1_\infty$ due to unmodeled factors such as sudden disturbances, change in surface friction coefficient, etc. In such a scenario, we would like to drive the state of the vehicle back into the mode 1 RCI set in a finite number of time steps. This leads to the notion of N–step backward reachable sets or N–step controllable sets.

Definition 5: The *N–step backward reachable sets* $\mathcal{Z}_N$ to a given target set $\mathcal{Z}$ are recursively defined as:

$$\mathcal{Z}_k = Pre(\mathcal{Z}_{k-1}), \quad (k = 1, ..., N), \quad \mathcal{Z}_0 = \mathcal{Z}. \tag{14}$$

If the state of the vehicle lies in $\mathcal{Z}_N$, there exists a sequence of control inputs $\{u(k)\}_{k=0}^{N-1}$ which ensures that the predicted state of the vehicle will lie inside the target set $\mathcal{Z}$ in N steps. We can compute $\mathcal{Z}_N$ by using Algorithm 1 (discussed in Section III-B) to recursively compute $Pre(\mathcal{Z}_k), (k = 0, ..., N)$. Figure 4 shows the 4–step backward reachable sets to $\mathcal{Z}^1_\infty$ for $\mu = 0.3$ and $v_x = 50$ kph. Note that $\mathcal{Z}_N$ is non–convex in general as it is a union of convex sets. We now define the control mappings corresponding to the k–step backward reachable sets.

Definition 6: The *control mapping* $\mathcal{U}_k(\cdot)$ *corresponding to* $\mathcal{Z}_k$ is defined as:

$$\mathcal{U}_k(z, \delta_d) := \{u : (z, u, \delta_d) \in \mathcal{Q}, z^+ \in \mathcal{Z}_{k-1}, \forall w_u \in \mathcal{W}_u(u)\}. \tag{15}$$

When the state of the vehicle goes outside the RCI set, our control strategy identifies the smallest k such that $z \in \mathcal{Z}_k$. For each $\delta_d \in \mathcal{W}_z(z)$, choosing any input from $\mathcal{U}_k(z, \delta_d)$ ensures that the predicted state of the vehicle will lie inside $\mathcal{Z}_{k-1}$. Repeating this procedure at every time step ensures that the controller will eventually drive the state back into $\mathcal{Z}_\infty^1$ in a finite number of time steps. Note that the analysis guarantees robustness to the uncertainty w_u as well as to the disturbance δ_d so long as the constraints $w_u \in \mathcal{W}_u(u)$ and $\delta_d \in \mathcal{W}_z(z)$ are satisfied.

B. Reachability analysis of the PWA bicycle model

We apply the algorithm developed in [7] for the robust reachability analysis of the PWA hybrid bicycle model with input and state–dependent disturbances. The algorithm for the computation of the one–step backward reachable set and RCI set can be derived in terms of set operations on the target set. The reader is referred to [7] for details of the proof. It is useful to define the following sets which represent state, input and disturbance constraints, and their projections:

$$\begin{aligned}\Omega := \{(z, u, \delta_d, w_u) : (z, u, \delta_d) \in \mathcal{Q}, \\ \delta_d \in \mathcal{W}_z(z), w_u \in \mathcal{W}_u(u)\} \subseteq \mathbb{R}^7, \end{aligned} \tag{16a}$$

$$\Omega_{z,u,\delta} := \text{Proj}_{z,u,\delta}(\Omega), \quad \Omega_{z,\delta} := \text{Proj}_{z,\delta}(\Omega),$$
$$\Omega_z := \text{Proj}_z(\Omega). \tag{16b}$$

The steps for the computation of $Pre(\mathcal{Z})$ are given by Algorithm 1. Based on this method, the iterative procedure to compute the mode 1 RCI set is given by Algorithm 2. Note

Algorithm 1 Pre set computation

1. $\Phi(\mathcal{Z}) = \{(z, u, \delta_d, w_u) \in \Omega : z^+ \in \mathcal{Z}\}$
2. $\Delta_1 = \Omega \backslash \Phi(\mathcal{Z})$,
3. $\Psi = \text{Proj}_{z,u,\delta}(\Delta_1)$,
4. $\Sigma_1 = \Omega_{z,u,\delta} \backslash \Psi$,
5. $\Sigma_2 = \text{Proj}_{z,\delta}(\Sigma_1)$,
6. $\Delta_2 = \Omega_{z,\delta} \backslash \Sigma_2$,
7. $\Delta_3 = \text{Proj}_z(\Delta_2)$,
8. $Pre(\mathcal{Z}) = \Omega_z \backslash \Delta_3$

Algorithm 2 RCI set computation

$i = 0$
$\mathcal{Z}_i = \mathcal{P}_1$
repeat
  $i = i + 1$
  $\mathcal{Z}_i = Pre^1(\mathcal{Z}_{i-1}) \cap \mathcal{Z}_{i-1}$
until $\mathcal{Z}_i == \mathcal{Z}_{i-1}$
$\mathcal{Z}_\infty^1 = \mathcal{Z}_i$

the use of $Pre^1(\mathcal{Z})$ instead of $Pre(\mathcal{Z})$ in Algorithm 2. This notation implies that we perform the one–step reachability analysis using the constraints and dynamics associated with mode 1 only. Figure 5 shows the output of Algorithm 2 for $\mu = 0.3$ and $v_x = 50$ kph. Since the model (7) is affine, and the state and input constraints are polyhedral, the sets

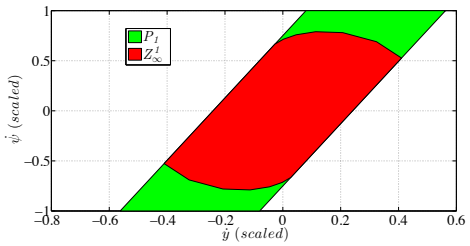

Fig. 5. Maximal RCI set $\mathcal{Z}_\infty^1$, $\mu = 0.3$, $v_x = 50$ kph.

$Pre(\mathcal{Z})$ and $\mathcal{Z}_\infty^1$ are also polyhedral by construction [7], [16]. The Multi–Parametric Toolbox (MPT) [17] in MATLAB can efficiently perform set operations on polytopes, and hence was used for the reachability analysis and RCI set computations.

C. Robust control design with reference tracking

The stability control system provides front steering corrections and yaw moment commands in order to track a given reference in the state–space. The reference signals, $r = [\dot{y}_{ref}, \dot{\psi}_{ref}]^T$, are a function of the current states and the driver's steering input. We use a standard reference generator for ESC systems [12] which is based on a steady–state cornering analysis of the linear bicycle model. The optimal control input, $u^\star = [\delta_{AFS}, M]^T$, is computed by minimizing a quadratic cost function as:

$$u^\star = \underset{u \in \mathcal{U}_\star(z,\delta_d)}{\arg\min} \; (z^+ - r)^T Q (z^+ - r) + (u - u_{pre})^T R (u - u_{pre}), \tag{17}$$

where Q and R are suitably chosen positive definite matrices, z^+ is the predicted state at the next time step given by model (7), and u_{pre} is the control input commanded at the previous time step. Depending on the current value of the state z, the set of admissible control inputs $\mathcal{U}_\star(z, \delta_d)$ is given by either (13) or (15). In particular, if $z \in \mathcal{Z}_\infty^1$, then $\mathcal{U}_\star(z, \delta_d) = \mathcal{U}_\infty^1(z, \delta_d)$, otherwise $\mathcal{U}_\star(z, \delta_d) = \mathcal{U}_k(z, \delta_d)$, where k is the smallest positive integer for which $\mathcal{U}_k(z, \delta_d)$ is not empty. Note that the controller is switched based on the polytopes $\mathcal{U}_\infty^1$ and $\mathcal{U}_k$ which are computed offline.

The cost function in (17) is used only when the vehicle is in mode 1 or when the front tires are not saturated. If the front tires are saturated, we impose a penalty on the high positive or negative slip angle in order to drive it to that value at which maximum lateral force is obtained. Since the AFS only provides control of the front slip angle, we ignore the rear slip angle in the modified cost function. In this case, we obtain the control input $u^\star$ as the optimizer of the following problem:

$$\begin{aligned} u^\star = \underset{u \in \mathcal{U}_\star(z,\delta_d)}{\arg\min} \; & (z^+ - r)^T Q (z^+ - r) \\ & + (u - u_{pre})^T R (u - u_{pre}) + P(\alpha_f^+ - \hat{\alpha}_f)^2, \end{aligned} \tag{18}$$

where $P > 0$, α_f^+ is the linear approximation of the predicted front slip angle at the next time step given by (3), and $\hat{\alpha}_f$ is the value of the front tire slip angle at which the lateral force is maximum. The definition of $\mathcal{U}_\star(z, \delta_d)$ is the same

as that for the optimization problem (17). The optimization problems (17) and (18) are quadratic programs as z^+ and α^+ are affine in u, and the sets $\mathcal{U}_\star(z, \delta_d)$ defining the constraints on u are polyhedral. Note that the optimal control input $u^\star$ has two components: *i*) the front wheel steering angle $u^\star(1)$ and *ii*) the yaw moment $u^\star(2)$. While we can directly set $\delta_{AFS} = u^\star(1)$, the yaw moment command must be converted to four individual braking torques that can be applied to the four wheels. The wheel braking torques are computed from $u^\star(2)$ using the algorithm presented in [8].

IV. Experimental Results

A. Experimental setup

The effectiveness of the proposed stability controller is demonstrated through tests on a prototype Jaguar S equipped with an AFS system and four wheel independent braking. The tests were performed through February and March 2012 at the Smithers Winter Test Center, Raco, Michigan, in collaboration with the Ford Motor Company. The body frame states (lateral and longitudinal velocity, and yaw rate) were measured by an Oxford Technical Solution (OTS) RT3002 sensing system, and the real–time computations were performed on a dSPACE© rapid prototyping system. The sampling time for all the experiments was $T_s = 0.05$s.

B. Results

We performed several tests on an icy surface ($\mu \approx 0.3$), and present the results from two relevant experiments in this work. In the first experiment, the driver performed a standard double lane change maneuver with an entry speed of 60 kph and maintained an almost constant position of the accelerator pedal. The tuning parameters are: N = 4; inside $\mathcal{Z}_\infty^1$, we set $Q = \text{diag}\,[0.1, 30]$ and $R = \text{diag}\,[2, 0.1]$; outside $\mathcal{Z}_\infty^1$, we set $Q = \text{diag}\,[0.1, 10]$ and $R = \text{diag}\,[2, 0.1]$, $P = 0.07$.

The vehicle response is shown in Figures 6–8. In Figure 6, we show the performance of the controller in tracking yaw rate and lateral velocity signals. We also compare the vehicle states with the controller being active to the states when the active safety system is disabled. We obtain a satisfactory tracking performance and are able to prevent the vehicle from attaining high values of lateral velocity and yaw rate.

In the upper plot of Figure 7, we plot the driver's steering input, the AFS command and the measured total front wheel steering angle. The controller imposes a counter–steering correction which results in vehicle stabilization. The AFS command is opposite to the driver's input in order to generate a counter–yaw moment to avoid a spin–out. In addition, the braking moment command supports this action as shown in the bottom part of Figure 7.

Figure 8 depicts the evolution of the state trajectory superimposed on the 3–step backward reachable set which were computed offline. The controller is able to compute an input command such that the vehicle states always lie in $\mathcal{Z}_\infty^1$.

The second experiment was performed on an icy circular track ($\mu \approx 0.2$) of diameter 110 m at a speed of approximately 40 kph. The aim of this test was to verify the controller action *i*) when the vehicle simultaneously

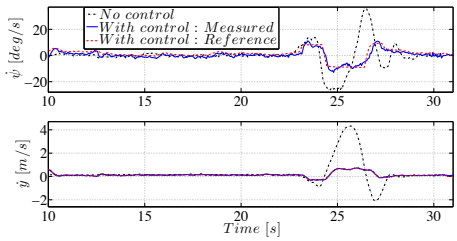

Fig. 6. Experiment 1: Tracking performance and comparison with case in which controller is disabled.

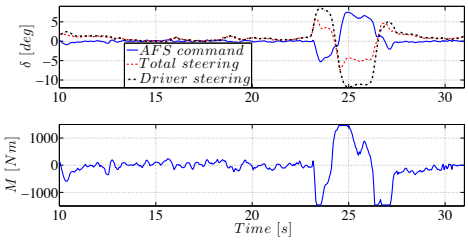

Fig. 7. Experiment 1: Driver steering profile and control inputs.

experiences front and rear tire saturation and *ii*) when model mismatch occurs as a result of any of the assumptions 1 and 2 not being satisfied. In particular, our control model assumes a friction coefficient of 0.3, which is different from the actual friction coefficient observed in this experiment. The tuning parameters are the same as those used in the first experiment. The vehicle response is shown in Figures 9–12.

Figure 10 shows the state trajectory superimposed on the 3–step controllable set. Although the state of the vehicle goes outside the mode 1 RCI set $\mathcal{Z}_\infty^1$, the controller is able to bring the state back into $\mathcal{Z}_\infty^1$ within a short time. In Figure 9, we note that the tracking performance is affected

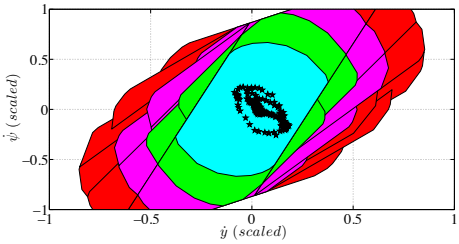

Fig. 8. Experiment 1: Evolution of state trajectory. The states always stay inside $\mathcal{Z}_\infty^1$.

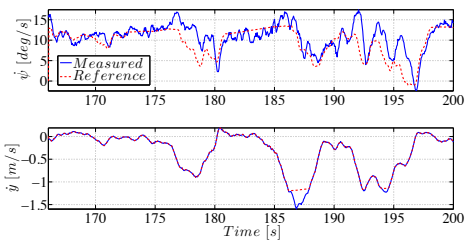

Fig. 9. Experiment 2: Tracking performance.

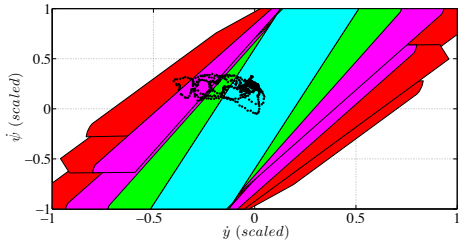

Fig. 10. Experiment 2: Evolution of state trajectory: state goes outside $\mathcal{Z}_\infty^1$ during circular maneuver.

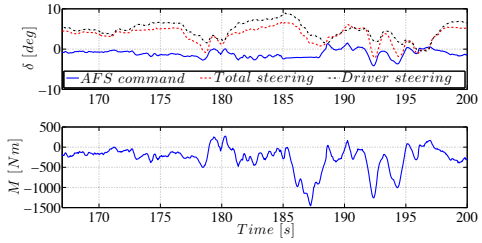

Fig. 11. Experiment 2: Driver steering profile and control inputs.

by the excursion of the state outside $\mathcal{Z}_\infty^1$. The main reason for the relatively poor tracking in such a situation is that the reference trajectory is generated using a steady–state cornering analysis.

We illustrate the effectiveness of using the modified cost function (18) in Figures 11 and 12. In the top part of Figure 11, we plot the driver's steering input, the AFS command and the measured total front wheel steering angle. Figure 12 shows that around $t = 185$s, the absolute values of both, the front and rear tire slip angles become greater than $\hat{\alpha}_f$ and $\hat{\alpha}_r$, respectively. In order to stabilize the vehicle in this case, the controller generates a negative yaw moment by the combination of a negative AFS command and a negative yaw moment command, as desired. This causes the front tire slip angle to return to the linear region at $t = 187$s.

V. Conclusions

In this paper, we presented the design of a robust vehicle stability controller which uses AFS and differential braking. The control approach explicitly considers the driver's intent in the control design process, taking into account the uncertainty in both, the driver behavior and the commanded input.

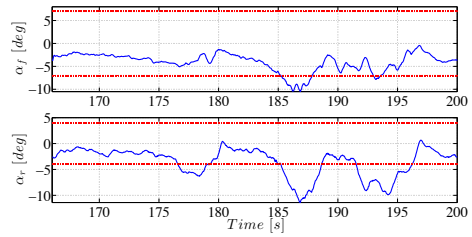

Fig. 12. Experiment 2: Computed front (top) and rear (bottom) slip angles. The dotted line denotes $\hat{\alpha}_\star$.

The experimental results illustrate the effectiveness of the proposed controller, which is able to guarantee convergence into the maximal RCI set despite model mismatch and the presence of state and input constraints.

VI. Acknowledgments

This material is based upon work supported by the National Science Foundation under Grant No. 1239323. Any opinions, findings, and conclusions or recommendations expressed in this material are those of the authors and do not necessarily reflect the views of the National Science Foundation. The authors thank Vladimir Ivanovic from the Ford Motor Company for his support during the experiments.

References

[1] Vehicle Dynamics Standards Committee, "Automotive stability enhancement systems," *SAE J1939*, 2004.

[2] J. Ackermann, D. Odenthal, and T. Bünte, "Advantages of active steering for vehicle dynamics control," in *Proceedings of 32nd ISATA, Automotive Mechatronics Design and Engineering*, 1999, pp. 263–270.

[3] S. Mammar and D. Koenig, "Vehicle handling improvement by active steering," *Vehicle System Dynamics*, vol. 38, no. 3, pp. 211–242, 2002.

[4] M. Nagai, M. Shino, and F. Gao, "Study on integrated control of active front steer angle and direct yaw moment," *JSAE review*, vol. 23, no. 3, pp. 309–315, 2002.

[5] G. Burgio and P. Zegelaar, "Integrated vehicle control using steering and brakes," *International Journal of Control*, vol. 79, no. 05, pp. 534–541, 2006.

[6] S. Di Cairano and H. Tseng, "Driver-assist steering by active front steering and differential braking: design, implementation and experimental evaluation of a switched model predictive control approach," in *Decision and Control (CDC), 2010 49th IEEE Conference on*. IEEE, 2010, pp. 2886–2891.

[7] G. Palmieri, M. Baric, L. Glielmo, E. Tseng, and F. Borrelli, "Robust vehicle lateral stabilization via set-based methods for uncertain piecewise affine systems: Experimental results," in *Decision and Control and European Control Conference (CDC-ECC), 2011 50th IEEE Conference on*. IEEE, 2011, pp. 3252–3257.

[8] P. Falcone, H. Tseng, F. Borrelli, J. Asgari, and D. Hrovat, "MPC-based yaw and lateral stabilisation via active front steering and braking," *Vehicle System Dynamics*, vol. 46, no. S1, pp. 611–628, 2008.

[9] F. Blanchini and S. Miani, *Set-theoretic methods in control*. Birkhäuser Boston, 2007.

[10] M. Barić, "Constrained control: Computations, performance and robustness," Ph.D. dissertation, ETH, 2008.

[11] S. Rakovic, M. Baric, and M. Morari, "Max-min control problems for constrained discrete time systems," in *Decision and Control (CDC), 2008 47th IEEE Conference on*. IEEE, 2008, pp. 333–338.

[12] U. Kiencke and L. Nielsen, *Automotive control systems: for engine, driveline, and vehicle*. Springer, 2005.

[13] R. Rajamani, *Vehicle dynamics and control*. Springer, 2011.

[14] H. Pacejka, *Tyre and vehicle dynamics*. Butterworth-Heinemann, 2005.

[15] W. Milliken, D. Milliken, and L. Metz, *Race car vehicle dynamics*. Sae International Warrendale, PA, 1995.

[16] S. Rakovic, E. Kerrigan, D. Mayne, and J. Lygeros, "Reachability analysis of discrete-time systems with disturbances," *Automatic Control, IEEE Transactions on*, vol. 51, no. 4, pp. 546–561, 2006.

[17] M. Kvasnica, P. Grieder, M. Baotić, and M. Morari, "Multi-parametric toolbox (MPT)," *Hybrid systems: computation and control*, pp. 121–124, 2004.